Marek MICHALCZUK[1], Bartłomiej UFNALSKI[2], Lech M. GRZESIAK[2], Piotr RUMNIAK[2]

Politechnika Warszawska, Instytut Automatyki i Robotyki (1), Instytut Sterowania i Elektroniki Przemysłowej (2)

Power converter-based electrochemical battery emulator

Abstract. *In this paper experimental assessment of converter-based emulator of voltage characteristics of electrochemical batteries is presented. The described emulator, which is part of the laboratory set for testing an electric vehicle powertrain system, allows to imitate an electrochemical energy storage. An AC grid supplied power electronic converter system enables to emulate both the battery discharge and charge modes. In order to emulate Li-ion battery behavior a mathematical model of a battery has been developed. The model of electrochemical cell has been created on the basis of the characteristics of Li-ion battery determined experimentally. Voltage characteristics take into account the change in battery voltage caused by state of charge, temperature and current. The model is dynamic, i.e. it reflects the transient state of battery output voltage.*

Streszczenie. *W artykule przedstawiono eksperymentalne wyniki dotyczące przekształtnikowego emulatora charakterystyk napięciowych baterii elektrochemicznych. Emulator, będący częścią stanowiska laboratoryjnego do badania układu napędowego pojazdu elektrycznego, pozwala na odwzorowanie elektrochemicznego magazynu energii. Przekształtnikowy układ zasilany z trójfazowego źródła sieciowego pozwala zarówno na emulacje baterii w trybie rozładowania, jak i ładowania. W celu odwzorowania baterii Li-ion opracowano jej model matematyczny. Model ogniwa elektrochemicznego wykonano na podstawie charakterystyk baterii Li-ion wyznaczonych doświadczalnie, uwzględniających zależność napięcia na zaciskach ogniwa od stanu jego naładowania, temperatury i natężenia prądu. Opracowany model jest modelem dynamicznym tj. odzwierciedla stany przejściowe napięcia wyjściowego baterii.* ***(Przekształtnikowy emulator baterii elektrochemicznych)***

Keywords: lithium-ion battery, dynamic battery model, battery emulator
Słowa kluczowe: bateria litowo-jonowa, model dynamiczny baterii, emulator baterii

doi:10.12915/pe.2014.07.03

Introduction

A battery emulator (BE) is a voltage source imitating the voltage at the terminals of an electrochemical battery during operation. Substitution of electrochemical cells with voltage source on a testbed of powertrain for electric vehicle allows a significant reduction of research cost. Energy storage is typically the most expensive part of electric vehicle powertrain. The use of the BE increases the flexibility of an experimental system [1, 2]. Batteries with different properties can be emulated without the need to swap battery cells in the system. Different states of battery, as state of charge, state of health and battery temperature can be changed directly without time-consuming preconditioning [3]. Moreover, the batteries need maintenance works as well as are affected by aging process. Therefore, in the future it would be required to replace batteries with a new ones to maintain the functionality of experimental system. Preliminary verification of control structure and exploratory evaluation of components for powertrain can be performed on the system, where battery cells have been replaced with the BE. Described emulator is a power electronic converter system that imitates battery behaviour by executing in real time the mathematical model of a battery.

The $LiFePO_4$ battery model is described in the next section. The following two sections show respectively the physical implementation of the emulator and experimental results.

Li-ion battery model

The lithium-ion battery model is based on data collected experimentally for WB-LYP40AHA cell of type $LiFePO_4$. In order to determine parameters of the cell, different discharging tests were conducted for various currents and temperatures. Each time after discharging test the battery was charged in CC-CV (constant current - constant voltage) mode with the current 5A and the voltage 3.6V at the temperature of 23°C. In the presented study, a temperature of electrodes measured at the terminals is considered as a battery temperature. In case of self-heating of the cell during discharge, an average temperature is taken into consideration. The dynamic characteristics of the battery pack are obtained by Thevenin-based model [4, 5, 6] shown in Figure 1, where U_{OCV} corresponds to an open circuit voltage of the battery and is a function of the state of discharge (SOD).

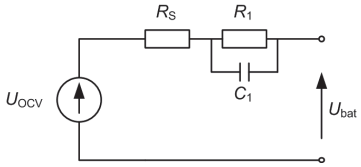

Fig. 1. Equivalent circuit of electrochemical battery

$$U_{\mathrm{OCV}} = f(\mathrm{SOD}) \tag{1}$$

The SOD is calculated by integrating the cell output current:

$$\mathrm{SOD}(t) = \frac{\int_0^t i(t)dt}{Q_{\max}} \cdot 100\% \tag{2}$$

with $\mathrm{SOD}(0) = 0$. A resistor R_{S} connected in series with a parallel RC branch models an ohmic drop and polarization effect [7].

Figure 2 shows voltages at the 40Ah battery terminals for the 20A pulse. Negative values of current indicate that battery is being discharged. Before the discharge pulse, battery output voltage U_{bat} depends on the current SOD. When battery discharge starts, an instant voltage drop U_{Ω} occurs. This drop is due to the internal resistance of the battery. Subsequently, the battery voltage is constantly decreasing, and evidently this decrease is greater than the voltage reduction resulting from increased SOD. A voltage decrease due to change in SOD is marked ΔU_1. The additional voltage drop results from polarization effect, which is connected with variations in reactant concentration at the electrodes. At the time of the stop of discharge, there is an immediate increase in battery voltage of value U_{Ω}, as a result of loss of voltage drop across the resistance. In the subsequent time the battery voltage slowly increases, which is the effect of gradually disappearing polarization voltage U_{P}. Finally, the battery voltage reaches a value resulting from the current SOD. Therefore, the output voltage of the battery U_{bat} is the sum of the open circuit voltage U_{OCV}, voltage across internal resistance U_{Ω} and polarization voltage U_{P}. Figure 3 shows the addends of the output voltage.

$$U_{\mathrm{bat}} = U_{\mathrm{OCV}} + U_{\Omega} + U_{\mathrm{P}} \tag{3}$$

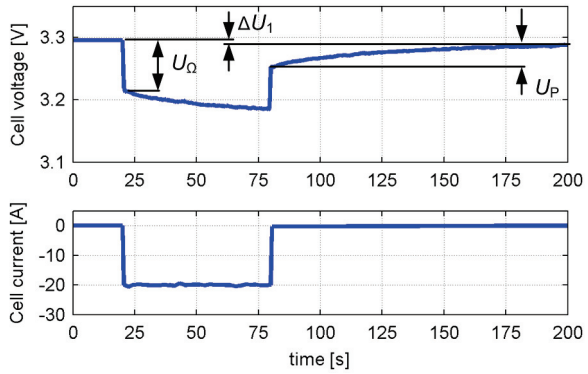

Fig. 2. Battery output voltage at pulse discharge of 20A

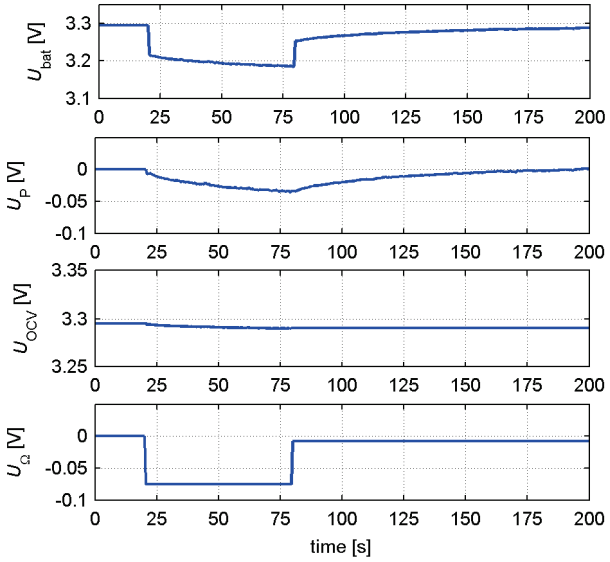

Fig. 3. Battery voltage and its addends during discharge pulse of 20A.

A charge pulse causes a similar change in the battery output voltage, with the difference that U_Ω and U_P are positive values. The internal series resistance R_S was determined according to the formula (4), through measuring the voltage drop (Fig. 2) on the battery terminals for a step change in the discharge current.

$$R_S = \frac{\Delta U_\Omega}{I} \tag{4}$$

The values of R_1 and C_1 (Fig. 1) have been determined by approximating U_P with a function of the form (5). Approximation has been made using Ezyfit toolbox in Matlab [8].

$$U_{\mathrm{P}}(t) = I \cdot R_1(1 - e^{-\frac{t}{R_1 \cdot C_1}}) \tag{5}$$

Voltage discharge characteristics of $LiFePO_4$ cell at different currents and temperatures are shown in Figure 4 and 5, respectively. With the increase of the discharge current the capacity of the cell decreases, as well as battery voltage at the terminals decreases due to voltage drop across the internal resistance. Low temperatures cause a significant decrease in capacity and an increase in internal resistance [9]. A nominal voltage of $LiFePO_4$ cells is 3.2V, and the cell voltage operating range is from 2.7V to 3.6V.

Figure 6 shows a schematic diagram of the battery model. All nonlinear dependencies have been modeled in one-dimensional lookup tables (1-D tables in Fig. 6). These

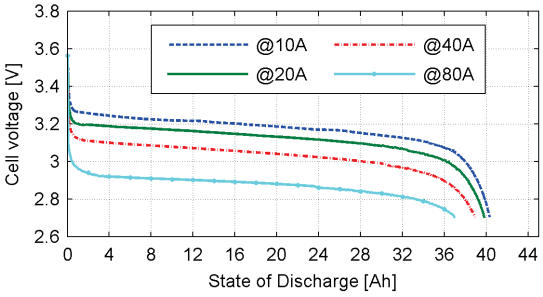

Fig. 4. Discharge characteristic of the Li-ion cell at the temperature of 23°C.

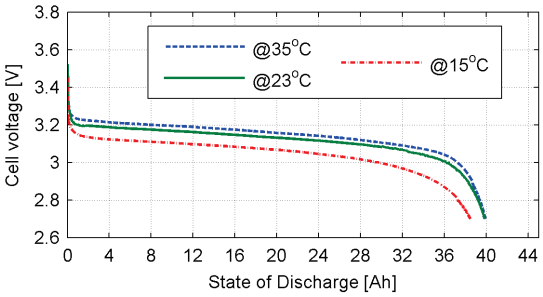

Fig. 5. Discharge characteristic of the Li-ion cell at the current of 20A.

blocks use linear interpolation to calculate the output values between recorded data points. The value of the open cell voltage $U_{\mathrm{OCV}}(\mathrm{SOC})$ has been determined on the basis of the discharge characteristics for 10A by adding a constant voltage drop [10]. An influence of a discharge current and a temperature on the cell capacity has been modelled by introducing factors k_1 and k_2 to equation (2).

$$\mathrm{SOD}(t) = \frac{\int_0^t k_1 \cdot k_2 \cdot i(t)dt}{Q_{\max}} \cdot 100\% \tag{6}$$

with $\mathrm{SOD}(0) = 0$.

The values of k_1 and k_2 factors (Fig. 7) have been determined from the final state of discharge ($\mathrm{SOD_f}$) for different currents and temperatures [11]. The k_1 factor is expressed as a function of a C-rate. The C-rate is a measure of the battery current relative to the maximum cell capacity. Discharging fully charged battery with 1C-rate means that the battery will be discharged in 1 hour.

$$k_1 = \frac{\mathrm{SOC_f}(I_n)}{\mathrm{SOC_f}(20)} \tag{7}$$

$$k_2 = \frac{\mathrm{SOC_f}(T_n)}{\mathrm{SOC_f}(23)} \tag{8}$$

The dependence of internal resistance R_s on temperature and SOC is implemented by using k_3 and k_4, and is illustrated in Figure 8. The change of open cell voltage depending on the temperature is shown in Figure 9. Constant entropy coefficient [12, 13] has been assumed, therefore the ΔU_T is approximated by a linear function.

$$\Delta U_T = 0.004456 \cdot T - 0.11478 \tag{9}$$

The constant parameters $\mathrm{R_{sn}}, \mathrm{R_{1n}}$ and $\mathrm{C_{1n}}$ in battery model were normalized to capacity of the cell of 40Ah (Table 1). Figures 10, 11 show k_5, k_7 and k_6, k_8 factors, which reflect a change of R_1 and C_1, respectively, as a function of temperature and SOC.

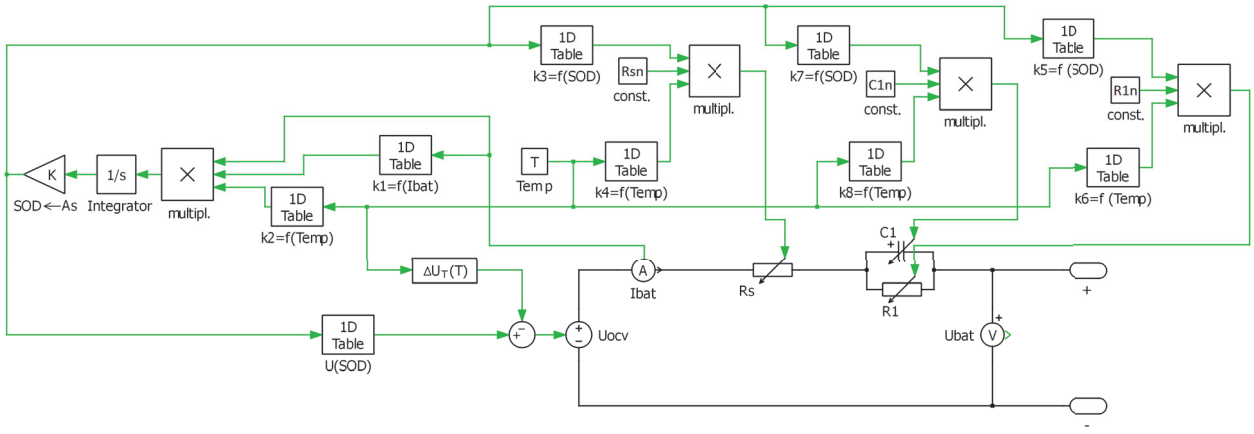

Fig. 6. Nonlinear mathematical model of the electrochemical battery

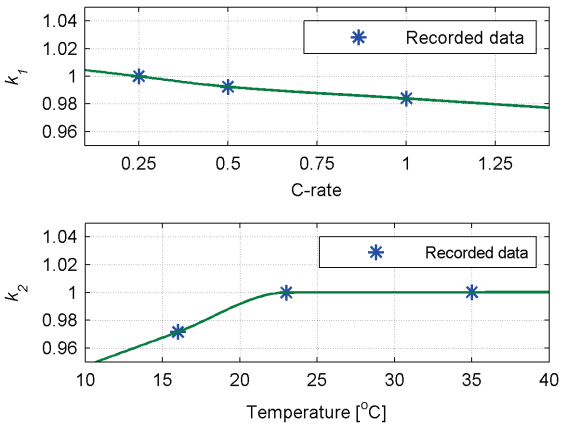

Fig. 7. The k_1 i k_2 factors as a function of battery current and temperature

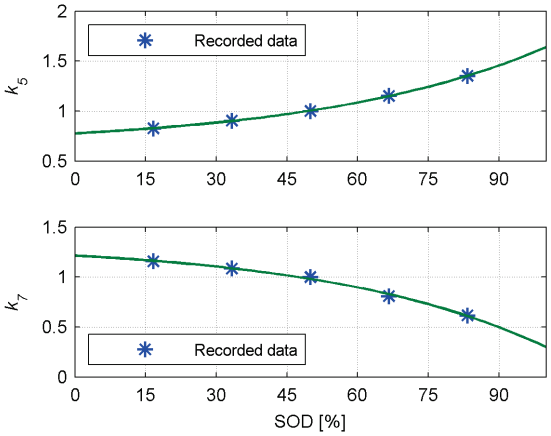

Fig. 10. The k_5 and k_7 factors characterizing R_1 and C_1 as a function of SOD

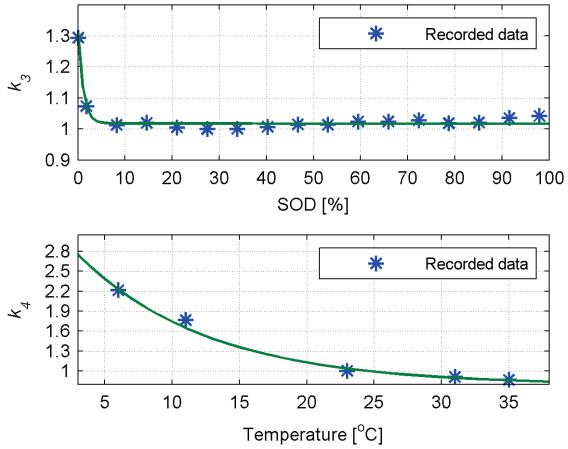

Fig. 8. The k_3 and k_4 factors characterizing change of R_s

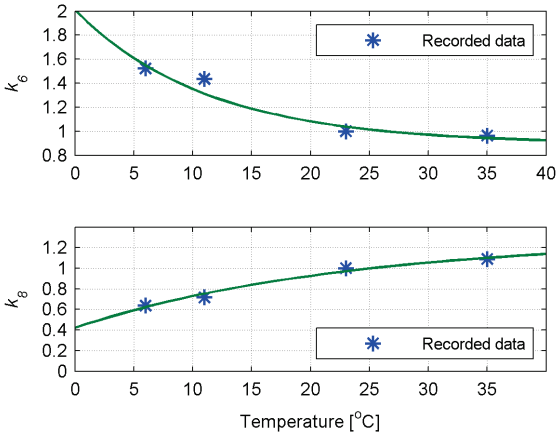

Fig. 11. The k_6 and k_8 factors characterizing R_1 and C_1 as a function of temperature

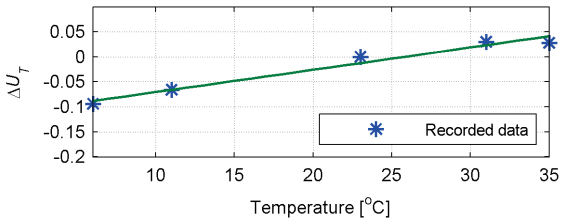

Fig. 9. The dependence of ΔU_T on temperature

Parameter	Value
R_{sn}	$\frac{3.1\mathrm{m\Omega}\cdot Q_{\mathrm{cell}}}{40\mathrm{Ah}}$
$R_{1\mathrm{n}}$	$\frac{1.9\mathrm{m\Omega}\cdot Q_{\mathrm{cell}}}{40\mathrm{Ah}}$
$C_{1\mathrm{n}}$	$\frac{22.75\mathrm{kF}\cdot Q_{\mathrm{cell}}}{40\mathrm{Ah}}$

Table 1. Constant parameters in the battery model

Battery emulator

A topology of the converter-based system developed to emulate voltage characteristics of electrochemical battery is shown in Figure 12. The converter system consists of two converters. The function of the BE is performed by the DC/DC converter. To ensure proper functionality of the BE a bidirectional source is required. The three-level grid converter is used as an interface to the three-phase grid in order to stabilize the DC-link voltage U_{DC1}. Voltage oriented con-

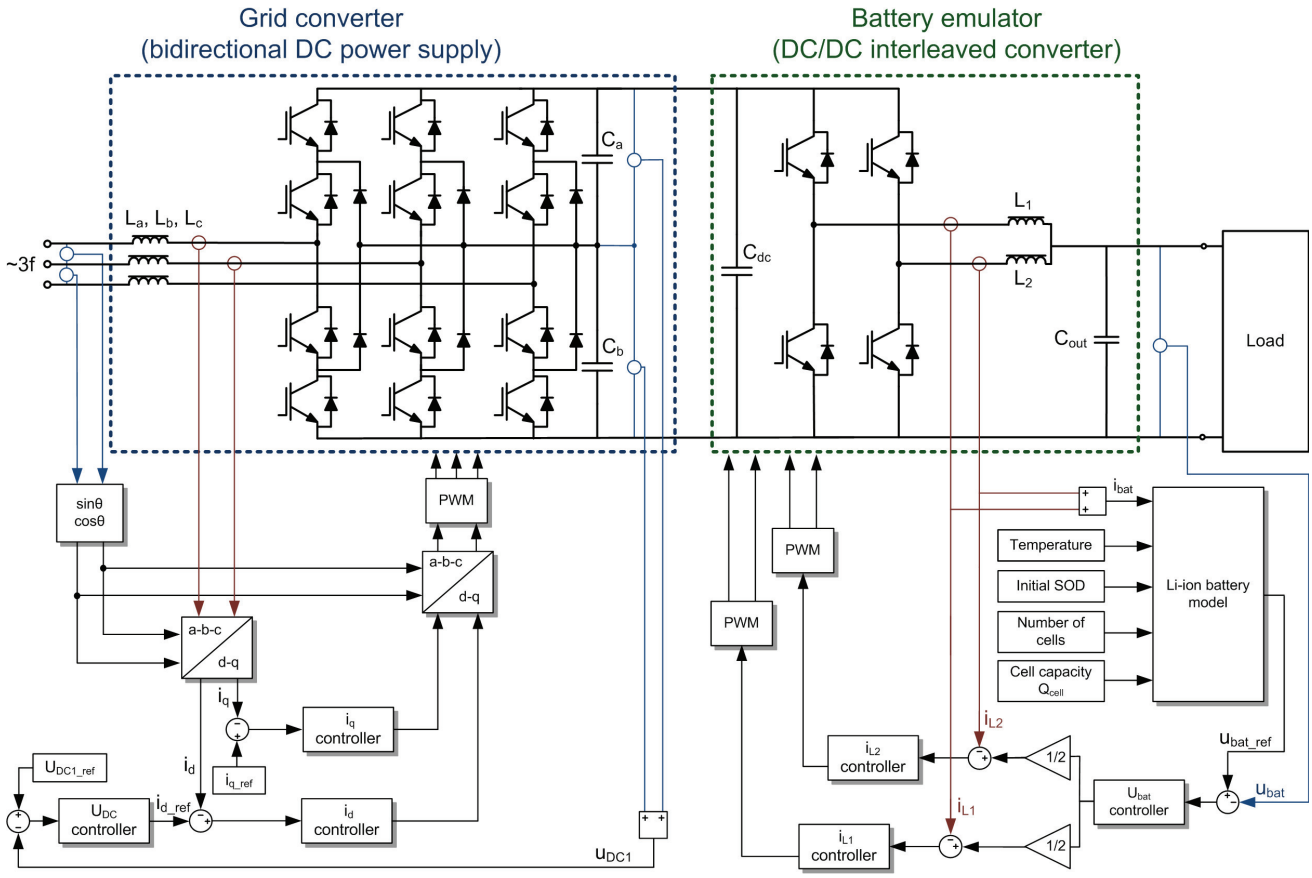

Fig. 12. Topology of the converter-based Li-ion battery emulator

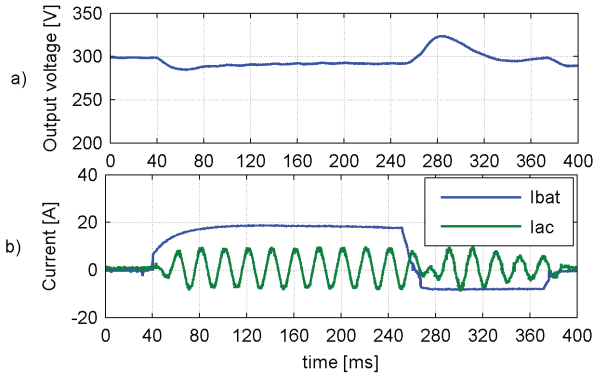

Fig. 13. The waveforms of the U_{DC1} voltage (a), phase current and the output current of the battery emulator (b)

trol (VOC) has been applied to control grid side converter [14, 15]. The VOC strategy uses two inner current control loops and an outer voltage control loop, all with PI controllers. The output of DC-link voltage controller is a value of reference current i_d^{ref}, which corresponds to the active power. The reference value of i_q^{ref} current, which corresponds to the reactive power, is set to zero to achieve unity power factor condition. The grid converter enables bidirectional energy flow to and from the grid. This allows charging and discharging battery mode emulation. Figure 13 shows a grid side converter output voltage and a phase current during charge and discharge pulses. A negative value of battery current i_{bat} corresponds to battery charging, resulting in energy flow to the grid.

The output stage converter is an interleaved step-down DC/DC converter with a common output capacitor providing the output voltage U_{bat} that is used to emulate the battery terminal voltage. The battery voltage U_{bat} is controlled

Parameter	Value
$L_{\mathrm{a}}, L_{\mathrm{b}}, L_{\mathrm{c}}$	1.5mH
L_1, L_2	1.0mH
C_{dc}	4mF
C_{out}	2.5mF
f_{switch}	20kHz
f_{sample}	10kHz

Table 2. Parameters of the battery emulator system

by cascade structure of controllers shown in Figure 12. A proportional-integral controller has been implemented to control output voltage. As a current controller a predictive controller, based on the mathematical model of DC/DC converter, has been implemented. Selected parameters of the converter system are listed in Table 2. The control algorithm has been implemented on two control boards with DSC TMS320F28335. Each converter has separate control board working independently. Total energy and voltage of the battery pack are predetermined by input parameters as the cell capacity and the number of cells in series.

Experimental results

Experiments have been conducted with emulator of a 6.4kWh $LiFePO_4$ battery. This energy storage has been emulated, based on introduced model, by 50 cells with a capacity of 40A connected in series. A nominal voltage of this battery pack is 160V. Figure 14 shows transient response for pulse discharge current. A step current causes battery voltage change as a composition of a step voltage drop and a first order transient response. The voltage drop amplitude and time constant vary with SOD and temperature.

The voltage of the battery pack is changing depending on SOD from 180V to 135V. As depicted in Figure 16, the output curves for various discharge currents show the lower voltage level, the higher is cell current. The effects of increased

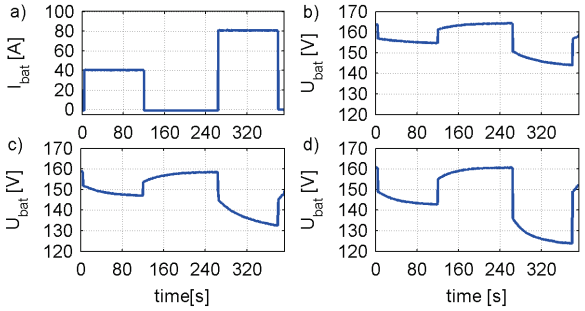

Fig. 14. Transient response for pulse current (a) at: 23°C and 10% SOD (b), 23°C and 80% SOD (c),10°C and 50% SOD (d)

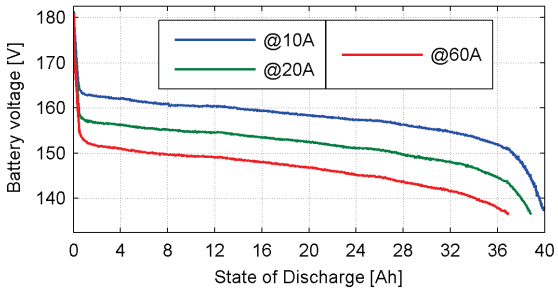

Fig. 15. Battery emulator voltage characteristics for various current battery at the temperature 23°C

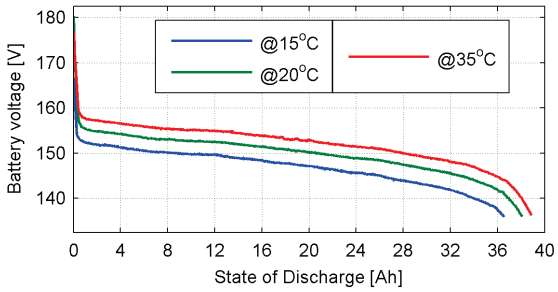

Fig. 16. Battery emulator voltage characteristics for various battery temperatures at the current of 40A

current are higher power losses as well as a decrease in capacity [16].

An electrochemical battery performance changes considerable with temperature. Figure 16 illustrates how the performance of lithium-ion batteries deteriorates as the operating temperature decreases. This results in a smaller capacity, a smaller energy efficiency and, what is more important in electric vehicle application, low power ability caused by increased voltage drop across internal resistance.

Conclusion

In the presented research the voltage characteristics of $LiFePO_4$ battery have been determined experimentally and the dynamic model of electrochemical battery has been developed. Based on the model created during the research, the control structure has been elaborated. The grid supplied system enables emulation of the electrochemical battery storage for laboratory drive systems. The developed power converter-based battery emulator imitates the battery terminal voltage depending on its state of charge and current drawn by a load. The presented system allows to emulate the battery voltage taking into consideration also various cell temperatures. The current version of battery model does not include thermal modeling, i.e. temperature parameter has to be introduced as a constant value. However, it is envisaged that such a functionality will be introduced in the next generation of the system. The emulator has been tested experimentally and its viability has been verified within the context of its suitability for electric powertrain system studies.

This study was financed from founds for statutory activity of Electric Faculty of Warsaw University of Technology. The funds has been provided under a grant titled "Sterowanie przepływem energii w pojeździe elektrycznym wyposażonym w baterię ogniw litowych i superkondensatory".

REFERENCES

[1] Baumhofer T., Waag W., and Sauer D.U. Specialized battery emulator for automotive electrical systems. In *IEEE Vehicle Power and Propulsion Conference (VPPC)*, pages 1–4, Sept. 2010.

[2] Mesbahi T., Rizoug N., Bartholomeus P., and Le Moigne P. Li-ion battery emulator for electric vehicle applications. In *IEEE Vehicle Power and Propulsion Conference (VPPC)*, pages 1–8, Oct. 2013.

[3] Konig O., Jakubek S., and Prochart G. Model predictive control of a battery emulator for testing of hybrid and electric powertrains. In *IEEE Vehicle Power and Propulsion Conference (VPPC)*, pages 1–6, Sept. 2011.

[4] Michalczuk M., Grzesiak L.M., and Ufnalski B. A lithium battery and ultracapacitor hybrid energy source for an urban electric vehicle. *Przegląd Elektrotechniczny (Electrical Review)*, 88(4b/2012):158–162, 2012.

[5] Rahmoun A. and Biechl H. Modelling of Li-ion batteries using equivalent circuit diagrams. *Przegląd Elektrotechniczny (Electrical Review)*, 88(7b/2012):152–156, 2012.

[6] Chulsung P., Jinfeng L., and Chou P.H. B#: a battery emulator and power-profiling instrument. *IEEE Design & Test of Computers*, 22(2):150–159, March 2005.

[7] Jian W., Jiang X., Zhang J., and Chen Y. Recursive adaptive parameters estimation for $LiFePO_4$ battery model. In *5th International Conference on Computational and Information Sciences (ICCIS)*, pages 1138–1141, 2013.

[8] Moisy F. *EzyFit – A free curve fitting toolbox for Matlab*, 2013. http://www.fast.u-psud.fr/ezyfit/.

[9] Jiayuan W., Zechang S., and Xuezhe W. Performance and characteristic research in LiFePO4 battery for electric vehicle applications. In *IEEE Vehicle Power and Propulsion Conference (VPPC)*, pages 1657–1661, 2009.

[10] Schonberger J. Modeling a lithium-ion cell using PLECS. Plexim GmbH, 2009.

[11] Lijun G., Liu S., and Dougal R.A. Dynamic lithium-ion battery model for system simulation. *IEEE Transactions on Components and Packaging Technologies*, 25(3):495–505, Sept. 2002.

[12] Eddahech A., Briat O., and Vinassa J.M. Thermal characterization of a high-power lithium-ion battery: Potentiometric and calorimetric measurement of entropy changes. *Energy*, 61:432–439, 2013.

[13] Zhang Z., Jia L., Zhao N., and Yang L. Thermal modeling and cooling analysis of high-power lithium ion cells. *Journal of Thermal Science*, 20(6):570–575, 2011.

[14] Dagbagi M., Hemdani A., Idkhajine L., Naouar M.W., Monmasson E., and Slama-Belkhodja I. FPGA-based real-time hardware-in-the-loop validation of a 3-phase PWM rectifier controller. In *IEEE Industrial Electronics Society IECON 39th Annual Conference*, pages 5374–5379, 2013.

[15] Mandiola J.F., Carmona D.C., Haghbin S., Abdulahovic T., and Ellsen M. An FPGA implementation of a voltage-oriented controlled three-phase pwm boost rectifier. In *IEEE Electrical Systems for Aircraft, Railway and Ship Propulsion (ESARS)*, pages 1–6, 2012.

[16] Pereirinha P. G., Trovao J. P., and Santiago A. Set up and test of a $LiFePO_4$ battery bank for electric vehicle. *Przegląd Elektrotechniczny (Electrical Review)*, 88(1a/2012):193–197, 2012.

***Authors**: mgr inż. Marek Michalczuk Instytut Automatyki i Robotyki,ul. Boboli 8, 02-525 Warszawa, E-mail: m.michalczuk@mchtr.pw.edu.pl; prof. dr hab. inż. Lech M. Grzesiak, dr inż. Bartłomiej Ufnalski, mgr inż. Piotr Rumniak, Instytut Sterowania i Elektroniki Przemysłowej, ul. Koszykowa 75,00-662 Warszawa, Polska.*